the plant journal

SEB Society for Experimental Biology

The Plant Journal (2017) **89,** 45–57 doi: 10.1111/tpj.13318

Electrostatic potentials of the *S*-locus F-box proteins contribute to the pollen *S* specificity in self-incompatibility in *Petunia hybrida*

Junhui Li[1,2], Yue Zhang[1,2], Yanzhai Song[1,2], Hui Zhang[1,2,†], Jiangbo Fan[1,2], Qun Li[1], Dongfen Zhang[1] and Yongbiao Xue[1,3,4,*]

[1]*State Key Laboratory of Molecular Developmental Biology, Institute of Genetics and Developmental Biology, Chinese Academy of Sciences and National Center for Plant Gene Research, Beijing 100101, China,*

[2]*University of Chinese Academy of Sciences, Beijing 100190, China,*

[3]*Beijing Institute of Genomics, Chinese Academy of Sciences, Beijing 100101, China, and*

[4]*Collaborative Innovation Center for Genetics and Development, Fudan University, Shanghai 200433, China*

Received 14 April 2016; revised 4 August 2016; accepted 22 August 2016; published online 14 November 2016.

*For correspondence (e-mail ybxue@genetics.ac.cn).

†Present address: College of Life Science, Northwest Normal University, Lanzhou 730070, China.

SUMMARY

Self-incompatibility (SI) is a self/non-self discrimination system found widely in angiosperms and, in many species, is controlled by a single polymorphic *S*-locus. In the Solanaceae, Rosaceae and Plantaginaceae, the *S*-locus encodes a single S-RNase and a cluster of *S*-locus F-box (SLF) proteins to control the pistil and pollen expression of SI, respectively. Previous studies have shown that their cytosolic interactions determine their recognition specificity, but the physical force between their interactions remains unclear. In this study, we show that the electrostatic potentials of SLF contribute to the pollen *S* specificity through a physical mechanism of 'like charges repel and unlike charges attract' between SLFs and S-RNases in *Petunia hybrida*. Strikingly, the alteration of a single C-terminal amino acid of SLF reversed its surface electrostatic potentials and subsequently the pollen *S* specificity. Collectively, our results reveal that the electrostatic potentials act as a major physical force between cytosolic SLFs and S-RNases, providing a mechanistic insight into the self/non-self discrimination between cytosolic proteins in angiosperms.

Keywords: self-incompatibility, SLF, pollen *S* specificity, electrostatic potentials, S-RNase, *Petunia hybrida*.

INTRODUCTION

Self and non-self recognition and discrimination are crucial to the survival of all living organisms ranging from bacteria to humans. They are involved in many biological events including immune defense and mate choice. In immune defense systems of both plants and animals, there are highly diverse receptor and ligand interactions occurring at cell membranes to distinguish self and non-self, for examples, trans-membrane pattern recognition receptors (PRRs) of host cells in plant and pathogen associated molecular patterns (PAMPs) of pathogen, inhibitory receptors at NK cell membrane and major histocompatibility complex (MHC) class I of normal cells, activating receptor NKG2D and stress inducible ligands of infect cells in innate immunity and T-cell receptors (TCRs) and peptides bound to MHC molecules (pMHC) in adaptive immunity (Boehm, 2006; Schwessinger and Ronald, 2012; Parham and Moffett, 2013; Rossjohn *et al.*, 2015). In addition to cell membranes, their specific interactions also occur in cytosols, for example, polymorphic NLR proteins and pathogen effectors (Jones and Dangl, 2006; Cui *et al.*, 2015). Self and non-self discrimination are also involved in mate choice. In flowering plants, one of the most important mate selection systems to prevent self-fertilization and to promote outcrossing is termed self-incompatibility (SI). SI allows the pistil to distinguish between genetically related (self) and genetically unrelated (non-self) pollen resulting in rejecting self but accepting non-self (De Nettancourt, 2001; Takayama and Isogai, 2005; Franklin-Tong, 2008; Zhang *et al.*, 2009). In most cases, SI is controlled by a single polymorphic *S*-locus encoding two major types of genes: the pistil *S* and the pollen *S* as the female and the male determinants of SI specificity, respectively. In Brassicaceae, the pistil SRK (*S*-locus receptor kinase) and the pollen *S*-locus cysteine-rich (SCR) interact at the plasma membrane of stigma papilla cell (Schopfer *et al.*, 1999; Takasaki *et al.*, 2000; Takayama *et al.*, 2001). In Papaveraceae, the

pistil PrsS and the pollen PrpS interact at the pollen tube plasma membrane (Foote *et al.*, 1994; Wheeler *et al.*, 2009). In the Solanaceae, Plantaginaceae and Rosaceae, the pistil S-RNase and the pollen *S* -locus F-box (SLF in the Solanaceae and Plantaginaceae, also called S-haplotype-specific F-box, SFB in the genus *Prunus* of the Rosaceae, or S-haplotype-specific F-box brothers, SFBB in the Maloideae of the Rosaceae) proteins interact in the cytosols of pollen tubes (Lee *et al.*, 1994; Murfett *et al.*, 1994; Lai *et al.*, 2002; Ushijima *et al.*, 2003; Qiao *et al.*, 2004a; Sijacic *et al.*, 2004; Takayama and Isogai, 2005; Sassa *et al.*, 2007; Zhang *et al.*, 2009; Liu *et al.*, 2014). Self-incompatibility in the Solanaceae, Plantaginaceae and Maloideae of Rosaceae are non-self recognition systems since there are multiple pollen *S* genes (SLF or SFBB) determining SI, whereas in *Prunus* of Rosaceae, there is only one pollen *S* gene (SFB) and the SI appears to be a self recognition system. Evolutionary analyses of pollen *S* indicate that *Prunus SFB* diverged early after the establishment of the Eudicots and originated in a recent *Prunus*-specific gene duplication event (Aguiar *et al.*, 2015; Akagi *et al.*, 2016).

Several models have been proposed to show how S-RNases and SLFs interact with each other to mediate their specific recognitions (Kao and McCubbin, 1996; Kao and Tsukamoto, 2004; Zhang *et al.*, 2009; Liu *et al.*, 2014). In the inhibitor model and S-RNase degradation model, a binding of specificity domains of self S-RNase and pollen *S* or SLF results in SI response, and interaction of the catalytic domain of non-self S-RNase and the inhibitor domain of pollen *S* or SLF leads to compatible response. Recently, a 'collaborative non-self recognition' system of S-RNase-based SI in Solanaceae was proposed, in which the product of each SLF interacts with a subset of non-self S-RNases, and the products of multiple SLF types are required for the entire collection of non-self S-RNases to be collectively recognized (Kubo *et al.*, 2010). Recent studies have shown two hypervariable regions of S-RNases, named HVa and HVb, are involved in their specificity and both regions are exposed on the protein surface (Matton *et al.*, 1997, 1999; Ida *et al.*, 2001; Matsuura *et al.*, 2001), and most positively selected sites are located in the HV regions of S-RNase of the Solanaceae, supporting an important role of the HV regions in their specific recognition (Vieira *et al.*, 2007; Brisolara-Correa *et al.*, 2015). SLF is an F-box protein with a conserved F-box domain at the N terminus. Most of F-box proteins usually serve as components of SCF (Skp1/Cullin/F-box) ubiquitin ligase complex that usually results in its target substrate polyubiquitination and degradation (Skaar *et al.*, 2013). Allelic SLFs are conserved proteins with low sequence variations (Ushijima *et al.*, 2003; Zhou *et al.*, 2003; Newbigin *et al.*, 2008), but two variable regions have been identified using Normed Variability Index (NVI) in SLF of *P. inflata* (Hua *et al.*, 2007), and only one variable region containing 27 amino acids has been identified in SFBB of Maloideae (Ashkani and Rees, 2016). Two variable (V1 and V2) and two hypervariable (HVa and HVb) regions have been identified in SFB of *Prunus* and they appear to be hydrophilic, which suggests that these regions may be exposed on the surface and function in the allele-specific recognition. In addition, positively selected sites appear to concentrate in these regions, further supporting that these regions could play an important role in the allele-specific recognition (Ikeda *et al.*, 2004; Nunes *et al.*, 2006). Recently, Hua *et al.* have divided PiSLF from *P. inflata* into three functional domains, FD1, FD2 and FD3, and shown that FD2 appears to function as an S-RNase-binding domain and FD1 and FD3 together likely determine its *S*-allele-specificity (Hua *et al.*, 2007).

In eukaryotes, it is known that several properties of protein-protein interfaces contribute to protein-protein interactions, such as complementarities between protein surfaces, residue interface propensities, hydrophobicity and conformational changes (Jones and Thornton, 1996; Sudha *et al.*, 2014). Structural approaches have shown that conformational changes are involved in the specific recognition of TCR and pMHC (Rudolph and Wilson, 2002; Rudolph *et al.*, 2006), and electrostatic forces, hydrophobic interactions, hydrogen bond and van der Waals contribute to the recognition of NB-LRR protein and pathogen effectors (Wang *et al.*, 2007; Dehury *et al.*, 2014). F-box proteins could recognize glycosylated proteins, and structural studies have identified a sugar-binding domain (SBD) in F-box protein Fbs1, which primarily recognize the disaccharide GlcNAc2 in the base of high mannose structure, and the binding site provides substrate specificity based on its shape and hydrogen-bonding network (Mizushima *et al.*, 2007). In addition, structural features of a specific conformation or assembly state could serve as recognition elements for F-box proteins. Polypeptides that fail to assume their native tertiary or quaternary structures are often subject to this mode of substrate recognition by F-box proteins and are ubiquitylated and degraded by the cytosolic proteasome (Hoseki *et al.*, 2010).

The physical interactions of the pistil and pollen *S* products allow self and non-self recognition and discrimination of pollen or pollen tubes, but their physical interacting forces remain obscure. In this study, we show that the electrostatic potentials of SLF protein surface contribute to the pollen *S* specificity through a physical mechanism of 'like charges repel and unlike charges attract' between SLFs and S-RNases in *P. hybrida.* Strikingly, alteration of a single C-terminal amino acid of SLF proteins reversed their surface electrostatic potentials and subsequently the pollen *S* specificity. Collectively, our results reveal that the electrostatic potentials act as a major physical force between cytosolic SLF and S-RNase proteins to contribute to the pollen *S* specificity, providing a mechanistic insight into

the physical force of self/non-self discrimination between cytosolic proteins.

RESULTS

Identification of one major region each from SLF and S-RNase involved in their physical interaction

To find out the proposed interaction domains of S-RNases and SLFs in *P. hybrida*, we first predicted the three-dimensional structural models of PhS_3-RNase and PhS_{3L}-SLF1 (PhS_9-SLF1), respectively, by I-TASSER. As for PhS_3-RNase structure prediction, the threading programs identified 1iooA (*Nicotiana alata* SF11-RNase) as the closest structural homologue and the predicted PhS_3-RNase structure had seven α-helices and four β-sheets (Figure 1a). To assess the quality and reliability of the modeled structure, the VADAR and ProSa-web were applied showing that the distribution of the ψ/φ angles of most amino acids (98%) was in the core and allowed region of the Ramachandran plot and Z-score (-6.96, 200aa) fell within the regions of experimentally solved structures of proteins with similar sizes (Figure S1). Furthermore, the structural comparison using the Dali server showed that the predicted PhS_3-RNase structure is similar to *N. alata* SF11-RNase (1ioo) and *N. glutinosa* ribonuclease NW (1iyb), suggesting it has a good homology with structures of T_2 RNase. As for PhS_{3L}-SLF1 structure prediction, the I-TASSER program generated top five models after iterative simulations. To determine the best model, C-score, folding energy and QMEAN norm score were examined (Table S1), and the final refined PhS_{3L}-SLF1 structure contained several α-helices in N-terminal and many β sheets in C-terminal (Figure 1a). To assess the quality of the modeled structure, similar VADAR and ProSa-web analyses were performed showing that the distribution of the ψ/φ angles of most amino acids (96%) was in the core and allowed region of the Ramachandran plot and Z-score (−5.45, 389aa) fell within the regions of experimentally solved structures of proteins with similar sizes (Figure S2). Furthermore, the structural comparison by Dali server showed that the predicted PhS_{3L}-SLF1 structure is similar to yeast Cdc4/Skp1 (3mksB), suggesting that it has a good homology with WD40-repeat β-propeller domain. These results together with a previous finding that two

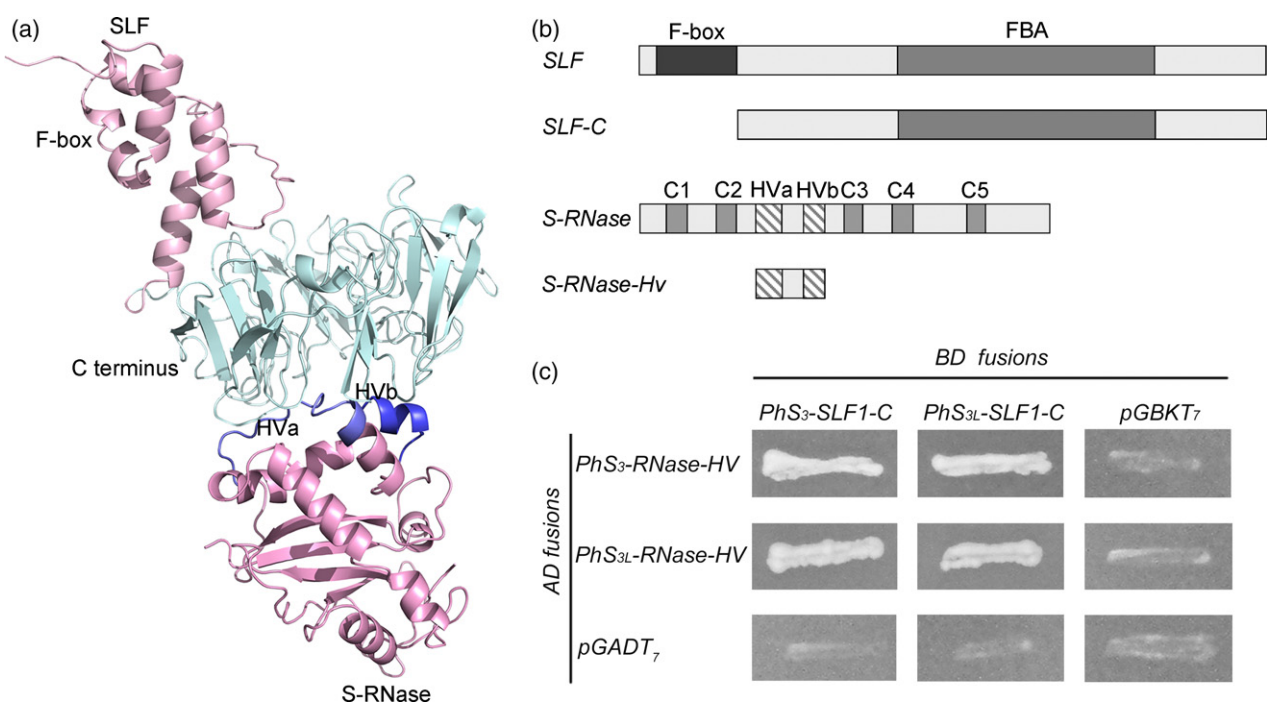

Figure 1. The C-terminal regions of PhSLFs interact with the hypervariable regions (HV) of PhS-RNases in yeast.
(a) A putative three-dimensional structural model of interaction of the C-terminal regions of SLFs and the hypervariable regions of S-RNases. The pink indicates the F-box domain, and the cyan the C-terminal regions of SLF proteins in top part, and the blue the hypervariable regions of S-RNases in bottom part.
(b) Schematic diagrams of *PhSLF* and *PhS-RNase* constructs used in yeast two-hybrid assays. SLF proteins contain one conserved F-box domain in their N-terminal and one FBA (F-box associated) domain in the C-terminal regions. C1, C2, C3, C4 and C5 indicate five conserved domains and HVa and HVb the hypervariable regions in S-RNases, respectively.
(c) Yeast two-hybrid assays of PhSLFs with PhS-RNases. The C terminal of PhS_3-SLF1 and PhS_{3L}-SLF1 were fused with BD and the hypervariable regions of S-RNase were fused with AD. The combinations of bait (BD fusion) and prey (AD fusion) constructs were introduced into the yeast strain AH109. Transformants were streaked on selective medium SD/-Ade-His-Leu-Trp and examined for growth. The empty vectors *pGBKT7* and *pGADT7* were used as negative controls. The plates were photographed after 7 days of incubation at 30°C.

hypervariable regions HVa and HVb of S-RNase play crucial roles in self/non-self-recognition suggest that the β-propeller-like domain of SLF and HV regions of S-RNase are likely involved in their interaction (Matton *et al.*, 1997). To validate the prediction, we performed a yeast two-hybrid assay and found that both the hypervariable regions of PhS_3-RNase and PhS_{3L}-RNase (PhS_9-RNase) interact with both the C-terminal regions of PhS_3-SLF1 and PhS_{3L}-SLF1 (Figure 1b,c), supporting that the long loop or α helixes structure in the hypervariable regions of S-RNase interacts with the top surface of the β-propeller-like domain in the C-terminal regions of SLF. The results of self and non-self interactions are consistent with the previous studies in yeast (Qiao *et al.*, 2004b; Liu *et al.*, 2014). Taken together, our results showed that one major region each from SLF and S-RNase is involved in their physical interaction, suggesting that surface properties of these regions appear to determine their recognition and interaction.

Electrostatic potentials form a major basis for the physical interaction between SLF and S-RNase

Surface electrostatic potentials and hydrophobicity are two critical factors in determining protein-protein interactions (Zhang *et al.*, 2011; Chanphai *et al.*, 2015). To identify which factor or both serve as a basis for the physical interaction between the major interacting regions of SLF and S-RNase, we first selected several SLFs and S-RNases from *P. hybrida* and *P. inflata* for which there are data for specific recognition from *in vivo* transgenic assay (Kubo *et al.*, 2010; Williams *et al.*, 2014) and predicted their surface electrostatic potentials. As shown in Figure 2, the negative electrostatic potentials of the C-terminal surfaces of PhS_5-SLF2 is consistent with the negative electrostatic potentials of the hypervariable regions of PhS_5-RNase and PhS_7-RNase, but opposite to the positive electrostatic potentials of the hypervariable regions of PhS_9-RNase and PhS_{11}-RNase, based on the principle of 'like charges repel and unlike charges attract,' the relationships of their surface charges are consistent with the recognition specificity of PhS_5-SLF2 and S-RNases *in vivo:* the transgene PhS_5-SLF2 caused the breakdown of SI in S_9 and S_{11} pollen, but not in S_5 and S_7 pollen (Kubo *et al.*, 2010) (Figure 2c). Similarly, the relationships of surface electrostatic potentials of PiS_2-SLF1 and different PiS-RNases, PiS_1-RNase, PiS_2-RNase, PiS_3-RNase, PiS_7-RNase are consistent with their recognition specificity *in vivo* based on the principle of 'like charges repel and unlike charges attract' (Williams *et al.*, 2014) (Figure 2d). Second, we predicted the surface hydrophobicities of these SLF and S-RNase proteins and found that there is little difference between the hypervariable regions of PhS_9-RNase and PhS_{11}-RNase which interacted with PhS_5-SLF2 and that of PhS_5-RNase and PhS_7-RNase which did not interact with PhS_5-SLF2. Similarly, there was not obvious correspondence between the surface hydrophobicities of PiS_2-SLF1 and different PiS-RNases, suggesting that there was little correlation

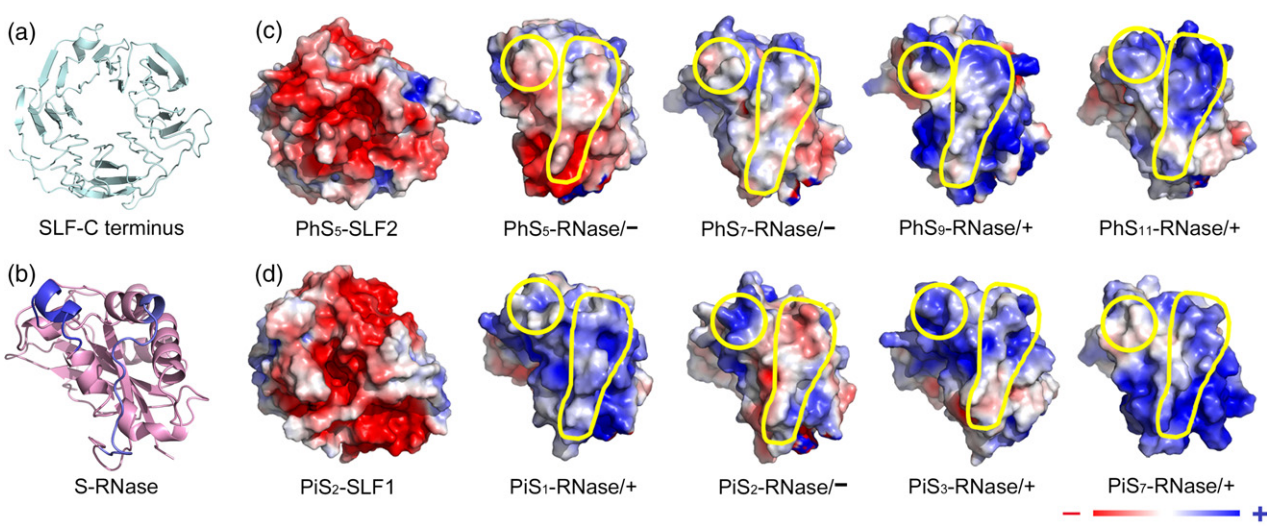

Figure 2. Surface electrostatic potentials of SLF and S-RNase proteins.
(a) A ribbon view of the C-terminus of SLF structure.
(b) A front side ribbon view of hypervariable regions of S-RNases, and blue indicates hypervariable regions of S-RNase.
(c) Surface electrostatic potentials of PhS_5-SLF2 and different S-RNases, PhS_5-RNase, PhS_7-RNase, PhS_9-RNase and PhS_{11}-RNase. The surface electrostatic potentials were calculated by PyMOL plug-in APBS tools, and blue indicates positive charge and red negative charge. The yellow irregular figures and circles indicate HVa and HVb regions of S-RNases, respectively. The plus sign '+' followed S-RNase represents there is interaction between PhS_5-SLF2 and this S-RNase, and the minus sign '−' no interaction between PhS_5-SLF2 and this S-RNase.
(d) Surface electrostatic potentials of PiS_2-SLF1 and different S-RNases, PiS_1-RNase, PiS_2-RNase, PiS_3-RNase and PiS_7-RNase. The plus sign '+' followed S-RNase represents there is interaction between PiS_2-SLF1 and this S-RNase, and the minus sign '−' no interaction between PiS_2-SLF1 and this S-RNase.

between the surface hydrophobicity and specific recognition of SLFs and S-RNases (Figure S3). To examine if electrostatic potentials are also involved in the physical interactions of additional SLFs and S-RNases, we further used more SLF and S-RNase proteins from *P. hybrida*, *P. inflata* and *P. axillaris* which had been shown for specific recognition from transgenic assays (Kubo *et al.*, 2010; Williams *et al.*, 2014) and predicted the electrostatic potentials of the C-terminal surfaces of SLFs and hypervariable regions of S-RNases, and analyzed the relationships of electrostatic potentials and their interactions of each pair of SLF and S-RNase proteins (Figures S17 and S18). The results showed the charge relationships of C-terminal domain of SLFs and HV regions of S-RNases of 62.2% pairs were consistent and 15.6% pairs partially consistent with their physical interactions (Table S7), suggesting that the electrostatic potentials play a major role in their specific physical interactions but there may be additional unknown physical forces such as complementarities between protein surfaces, residue interface propensities, conformational changes, hydrogen bond and van der Waals interactions involved in the physical interactions of S-RNases and SLFs. Taken together, these results suggest that the electrostatic potentials of SLF and S-RNase proteins could serve as a major basis for their physical interactions.

The C-terminal domain of PhSLF acts as a major specificity domain *in vivo*

To examine whether the major interaction regions of SLF with S-RNase are the specificity domains *in vivo*, we performed the domain-swapping transgenic experiments. Previously, Liu *et al.* introduced *PhS$_{3L}$-SLF1* into *S$_3$S$_{3L}$* plants, and *PhS$_{3L}$-SLF1* caused breakdown of SI in transgenic *S$_3$* pollen due to competitive interaction but no competitive interaction observed between *PhS$_3$-SLF1* and the *S$_3$* locus (Liu *et al.*, 2014). Thus, we divided PhS$_{3L}$-SLF1 and PhS$_3$-SLF1 into three domains based on their predicted structures, and swapped their corresponding domains and six chimeric PhSLFs (L-3-3, 3-L-L, 3-L-3, L-3-L, 3-3-L and L-L-3, where 3 and L represent the regions derived from PhS$_3$-SLF1 and PhS$_{3L}$-SLF1, respectively) were subsequently generated (Figure 3a,b), and after introduction of the chimeric PhSLFs driven by a native promoter of *PhS$_3$A-SLF1* into *P. hybrida* of *S$_3$S$_{3L}$* genotype, three to six independent transgenic lines were obtained and the expression of each transgene in pollen was confirmed by reverse transcription polymerase chain reaction (RT-PCR) analysis (Figure S4). To test the function of six chimeric SLFs *in vivo*, we performed self-pollination of the transgenic lines and found that the lines expressing the L-3-3 and L-L-3 chimeric proteins remained self-incompatible (Figure 3c,g and Table S2), indicating that both of them did not breakdown SI of *S$_3$* and *S$_{3L}$* pollen, whereas the transgenic lines carrying the transgenes *3-L-L*, *3-L-3*, *L-3-L* or *3-3-L* exhibited SI breakdown (Figure 3d–f,h and Table S2), and reciprocal crosses with wild-type *S$_3$S$_{3L}$* plants showed that the transgenes of *3-L-L*, *3-L-3*, *L-3-L* or *3-3-L* caused breakdown of pollen, but not style, function in SI (Figure S5), showing that these four chimeric genes are functional *in vivo.*

To determine whether breakdown of SI resulted from competitive interaction, we examined the inheritance of the *3-L-L*, *3-L-3*, *L-3-L* and *3-3-L* transgenes and *S* genotypes of progeny generated from self-pollination, and PCR analysis revealed that all progeny plants examined carried the transgenes and were either *S$_3$S$_3$* or *S$_3$S$_{3L}$*, and the observed segregation ratio of *S$_3$S$_3$* and *S$_3$S$_{3L}$* fit the expected segregation ratio 1:1 by chi-square test (Figures 3i, S6–S9 and Table S3), showing that they breakdown SI by competitive interaction and the absence of an *S$_{3L}$S$_{3L}$* genotype suggested that only *S$_3$* pollen, but not *S$_{3L}$* pollen, carrying the transgene became compatible with pistils of transgenic T_0 lines. Collectively, these results showed that the C-terminal region containing SIII domain of PhSLFs acts as a major specificity domain *in vivo.*

A single amino acid histidine is capable of determining the pollen *S* specificity *in vivo*

In order to determine which amino acid (s) in the C-terminal domain mediates the specificity of SLF *in vivo*, we first estimated selective pressure of each amino acid site of SLF. We used a total of 21 Type-1 SLFs from *P. inflata*, *P. hybrida* and *P. axillaris* to construct a phylogenetic tree to estimate the selective pressure of each amino acid site of them by PAML (phylogenetic analysis by maximum likelihood) (Table S4 and Figure S10a), and found that site 293 of SLF with dN/dS of 4.81 and NEB (Naive Empirical Bayes) probabilities of 0.996 and site 317 with dN/dS of 4.642 and NEB probabilities of 0.952 have been subjected to significantly positive selection (Figure S11). The site 317 of PhS$_3$-SLF1 and PhS$_{3L}$-SLF1 are both lysine (K), but the site 293 of PhS$_3$-SLF1 and PhS$_{3L}$-SLF1 are histidine (H) and glutamic acid (E), respectively, and the predicted structures revealed that 293 sites located on the C-terminal top surface as an interaction surface with S-RNases (Figure 4a), suggesting that site 293 is likely involved in the specific recognition of SLF and S-RNase. To examine this possibility, we swapped the site 293 between PhS$_3$-SLF1 and PhS$_{3L}$-SLF1, termed H293E and E293H, respectively, and compared their surface electrostatic potentials and found that the positive electrostatic potentials on the 293 site of PhS$_3$-SLF1 changed into the negative electrostatic potentials of H293E, and the negative electrostatic potentials on the 293 site of PhS$_{3L}$-SLF1 changed into neutral electrostatic potentials of E293H (Figure 4a), supporting a role of amino acid site 293 in the specificity of SLF by affecting the electrostatic potentials.

To examine their *in vivo* functions, *H293E* and *E293H* driven by the native promoter of *PhS$_3$A- SLF1* were

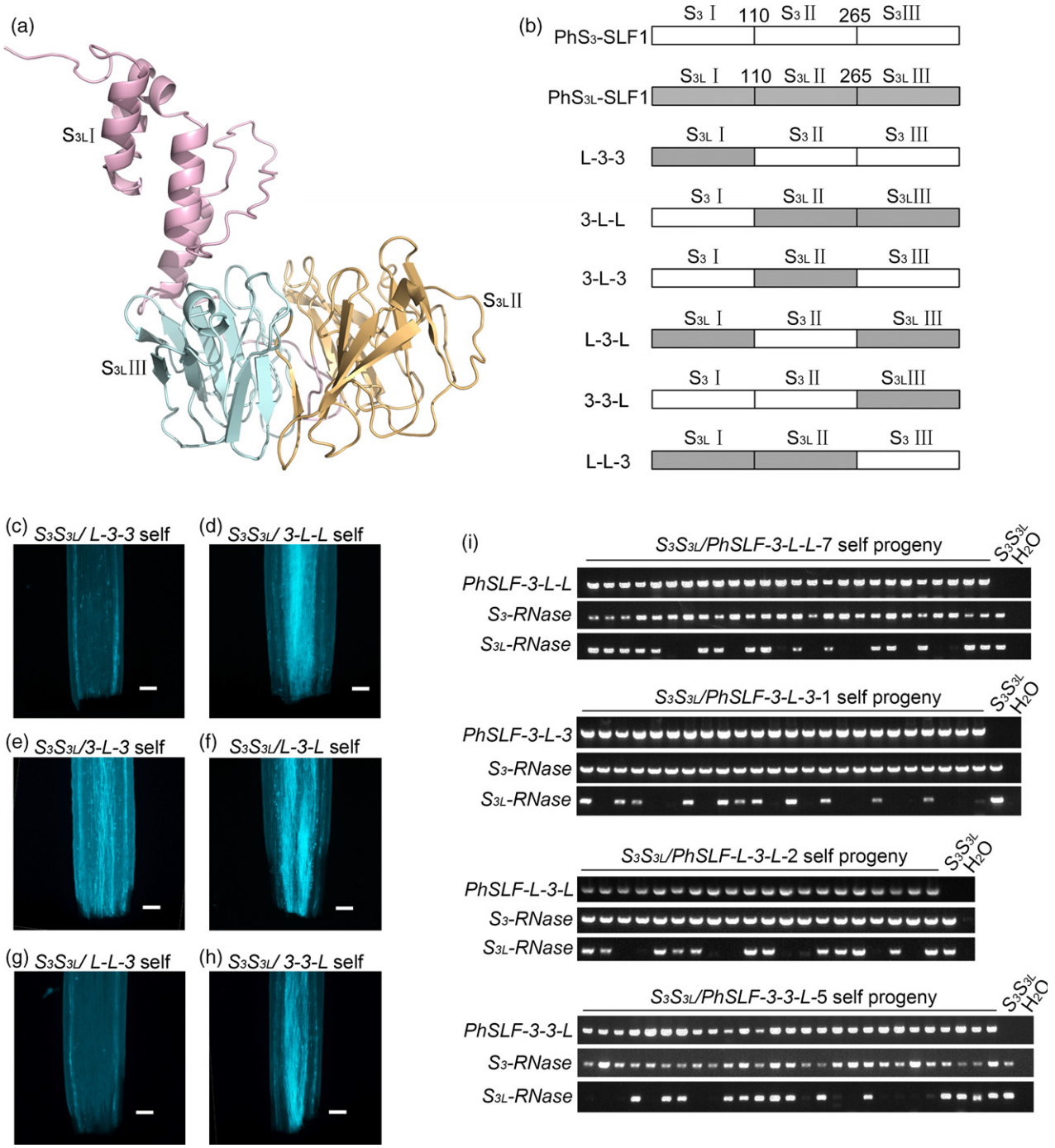

Figure 3. The C-terminal regions of PhSLFs are involved in the pollen *S* specificity.
(a) The putative 3D structure of PhS_{3L}-SLF1 protein. Pink helices indicate S_{3L}I domain composed of 1–109 amino acid residues, yellow sheets S_{3L}II domain of 110–264 amino acid residues, and cyan sheets S_{3L}III domain of 265–389 amino acid residues, respectively.
(b) Schematic representations of PhS_3-SLF1, PhS_{3L}-SLF1 and six domain-swapped chimeric proteins between them.
(c–h) *In vivo* pollination assays of transgenic plants of six chimeric *SLFs*. Pollen tubes were stained with aniline blue and monitored by a fluorescence microscope. Presence of a large number of pollen tubes at the basal end of the style indicates compatible pollinations. Transgenic plants S_3S_{3L}*/L-3-3* and S_3S_{3L}*/L-L-3* are self-incompatible. Transgenic plants S_3S_{3L}*/3-L-L*, S_3S_{3L}*/3-L-3*, S_3S_{3L}*/L-3-L* and S_3S_{3L}*/3-3-L* exhibit breakdown of SI. Scale bar represents 200 μm.
(i) Progeny genotype analysis of self-pollinated transgenic T_0 plants S_3S_{3L}*/3-L-L*, S_3S_{3L}*/3-L-3*, S_3S_{3L}*/L-3-L* and S_3S_{3L}*/3-3-L*. Primer pairs specific to S_3*-RNase* and S_{3L}*-RNase* were used for PCR amplification to identify the corresponding *S*-haplotype, respectively. Transgenes of chimeric *PhSLFs* were validated by its forward primer and *NOS*-terminator reverse primer. S_3S_{3L} and H_2O indicate negative control of wild-type and water, respectively.

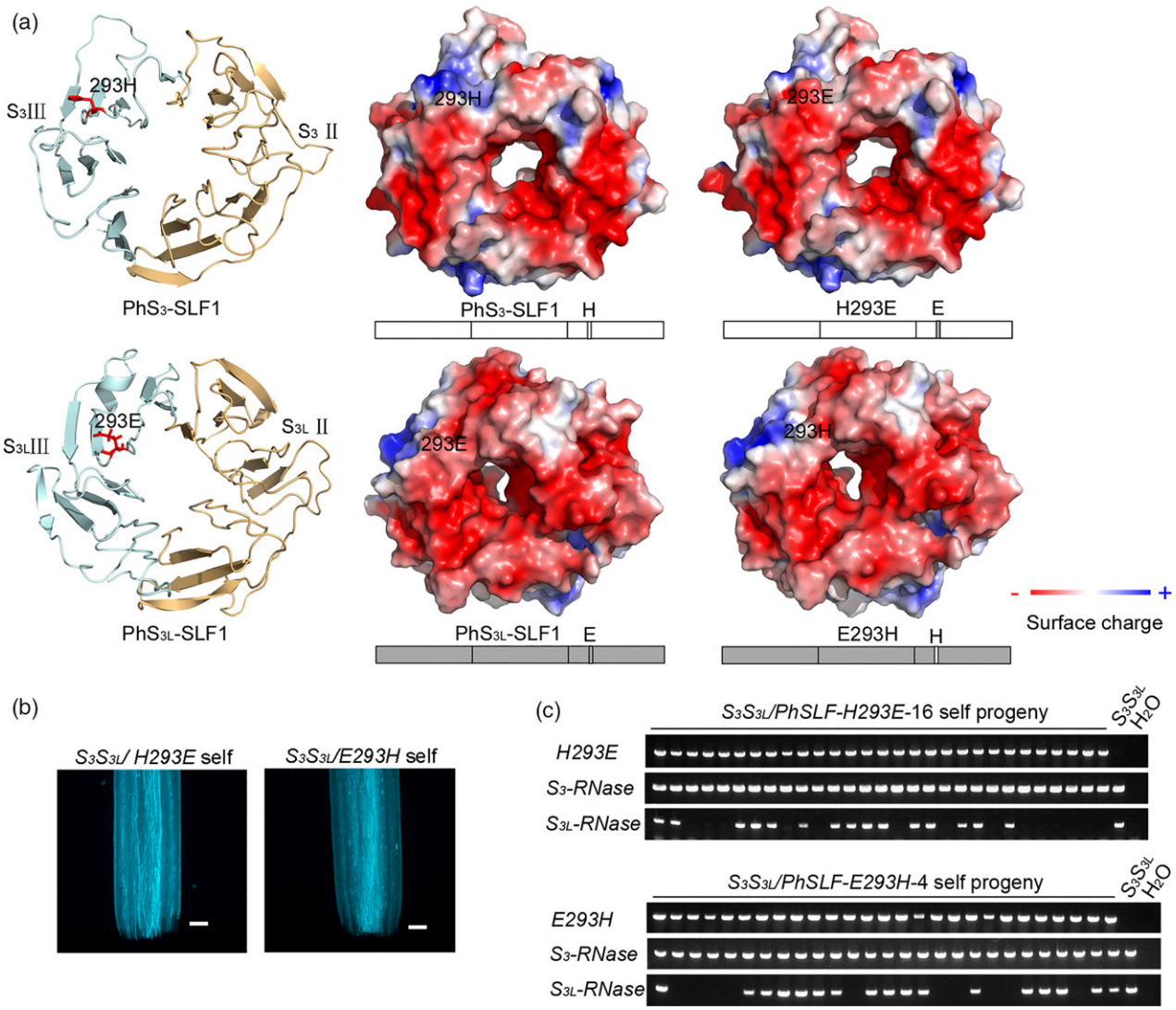

Figure 4. Reverse of the electrostatic potentials of SLF protein surface by a single C-terminal amino acid site 293 mutation alters the pollen *S* specificity.
(a) Predicted effects of 293 point mutations on surface electrostatic potential of PhS_3-SLF1 and PhS_{3L}-SLF1. Left column show top cartoon views of the C-terminal regions of PhS_3-SLF1 and PhS_{3L}-SLF1. The site 293 of PhS_3-SLF1 and PhS_{3L}-SLF1 are indicated by red sticks. Middle column show the electrostatic potentials of the C-terminal top surfaces of PhS_3-SLF1 and PhS_{3L}-SLF1, and right column of site 293 mutated SLFs. The surface electrostatic potentials were calculated by PyMOL software and blue indicates positive charge and red negative charge. The mutated amino acids are indicated on the protein structures. Schematic diagrams of the site 293 mutations of PhS_3-SLF1 and PhS_{3L}-SLF1 are shown under the protein structures, respectively. H, histidine; E, glutamate. Two point mutations were obtained after exchanging site 293 of PhS_3-SLF1 and PhS_{3L}-SLF1, termed H293E and E293H, respectively.
(b) *In vivo* pollination assays of transgenic plants of two site 293 mutated *SLFs.* Transgenic plant S_3S_{3L}*/H293E* and S_3S_{3L}*/E293H* exhibited breakdown of SI. Scale bar represents 200 μm.
(c) Progeny genotype analysis of self-pollinated transgenic T_0 plants S_3S_{3L}*/H293E* and S_3S_{3L}*/E293H.* Primer pairs specific to S_3*-RNase* and S_{3L}*-RNase*, respectively, were used for PCR amplification to identify the corresponding *S* haplotypes, respectively. Transgenes of site mutated *PhSLFs* were validated by its forward primer and *NOS*-terminator reverse primer. S_3S_{3L} and H_2O indicate negative control of wild-type and water, respectively.

introduced into *P. hybrida* of S_3S_{3L} genotype and the transgenic lines carrying transgenes *H293E* and *E293H* caused the breakdown of SI in pollen S_3 (Figures 4b,c and S12–S15 and Tables S5 and S6), showing that self SLF (PhS_3-SLF1) was reversed to non-self SLF (H293E) by the alteration of a single amino acid site reversing its surface electrostatic potentials, and non-self SLF (PhS_{3L}-SLF1) was not reversed to self SLF by the alteration of this single amino acid site, suggesting that there are other amino acids involved in the specificity of SLF. Based on the 'collaborative non-self recognition' system that the products of multiple SLF types are required to collectively recognize the entire collection of non-self S-RNases, we used a total of 17 SLFs of S_9 haplotype from *P. hybrida* to construct a phylogenetic tree to estimate the selective pressure of each amino acid site of them by PAML (Table S4 and Figure S10b), and found that 11 sites were subjected to positive selections with dN/dS of 1.804 to 2.516 and NEB

probabilities of 0.409 to 0.795, suggesting that these amino acid sites may also be involved in the specificity of SLF (Figure S16). Taken together, a single amino acid histidine in the C-terminal domain is capable of determining the pollen *S* specificity *in vivo* by reversing its electrostatic potentials.

To examine if the electrostatic potentials of site 293 and SIII domain of other SLFs contribute to their physical interacting force with S-RNases, we still used those SLF and S-RNase proteins which had been shown for specific recognition from transgenic assays (Kubo *et al.*, 2010; Williams *et al.*, 2014) and predicted the electrostatic potentials of the site 293 and the SIII domain of SLFs and hypervariable regions of S-RNases, and analyzed each pair of SLF and S-RNase proteins (Figures S17 and S18). The results showed the charge relationships of site 293 of SLFs and HV regions of S-RNase of 60% pairs were consistent and 20% pairs partially consistent with their physical interactions, and the charge relationships of the SIII domain of SLF and HV regions of S-RNase of 64.4% pairs were consistent and 15.6% pairs are partially consistent with their physical interactions (Table S7), suggesting that the electrostatic potentials of site 293 and SIII domain of SLFs play a major role in their specific physical interactions with S-RNase and there may be additional unknown physical forces involved in the specific interactions of S-RNases and SLFs.

SI breakdown of the transgenic S_3 pollen is associated with S_3-RNase polyubiquitination

Previous studies have shown that pollen SI breakdown by heteroallelic *SLFs* is mediated by polyubiquitination of S-RNases (Qiao *et al.*, 2004b; Entani *et al.*, 2014; Liu *et al.*, 2014). To examine the biochemical basis of SI breakdown of S_3 pollen by the chimeric *SLFs*, we selected transgenic pollen that expressed *S_{3L}-SLF1:FLAG*, *3-3-L:FLAG* and *H293E:FLAG* which represented three classes of transgenic constructs, respectively, and used their extracts for ubiquitination assay. To detect the expression of FLAG-tagged S_{3L}-SLF1, 3-3-L and H293E protein in pollen of S_3S_{3L} heterozygote, immunoblot analysis of immunoprecipitates by anti-FLAG antibody from non-transformed wild-type S_3S_{3L} pollen (WT) and transformed pollen expressing *S_{3L}-SLF1:FLAG*, *3-3-L:FLAG* and *H293E:FLAG* were performed and the S_{3L}-SLF1:FLAG,3-3-L:FLAG and H293E:FLAG proteins were expressed in transformed pollen tubes but not non-transformed wild-type S_3S_{3L} pollen tubes (Figure S19). Both oligo- and poly-ubiquitinated S_3-RNases were detected by both anti-S_3-RNase and anti-Ub antibodies, indicating that they were ubiquitinated by the three different SLFs (Figure 5a). The ubiquitination of S_3-RNase by H293E detected by anti-S_3-RNase was not strong as compared to that by S_{3L}-SLF1 and 3-3-L. This may be due to a difference in affinity between the S_3-RNase and different SLFs. By contrast, the ubiquitination of S_3-RNases did not occur in the immunoprecipitate of wild-type pollen extract (Figure 5a), indicating that S_{3L}-SLF1, 3-3-L and H293E is essential for the ubiquitination of S_3-RNase. The ubiquitinated S_{3L}-RNases were not detected by both anti-S_{3L}-RNase and anti-Ub antibodies, indicating that they were not ubiquitinated by the three different SLFs (Figure 5b). We detected S-RNases of approximately 55kD likely represented S_3-RNase and S_{3L}-RNase dimers because they were only detected by anti-S-RNase antibodies (Figure 5a,b). Taken together, these results showed that the protein products from three *SLFs*, *S_{3L}-SLF1*, *3-3-L* and *H293E* could

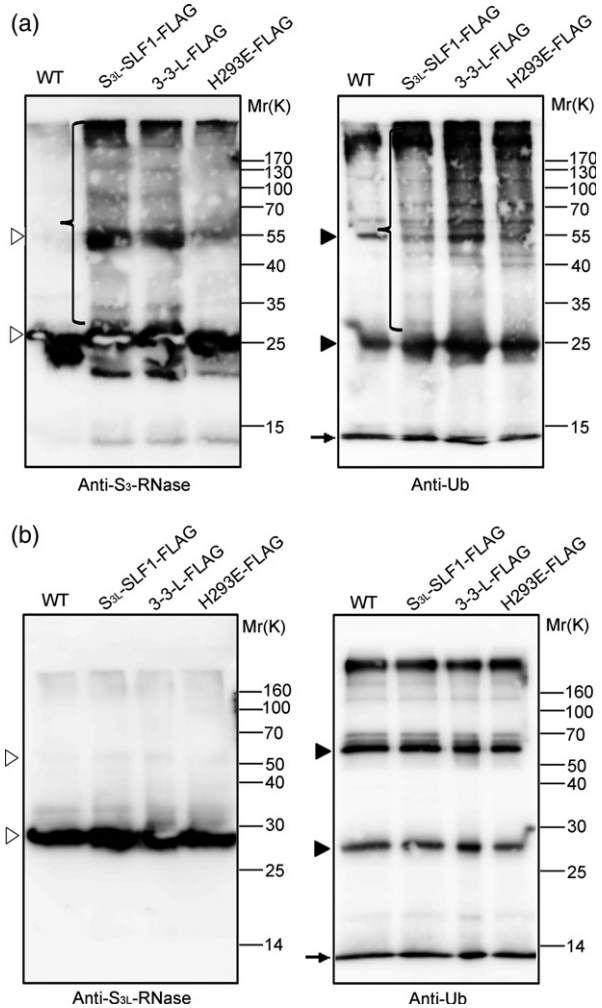

Figure 5. S_{3L}-SLF1, 3-3-L and H293E can form separate SCF complexes to poly-ubiquitinate S_3-RNases, but not S_{3L}-RNases.
(a, b) Immunoblot analysis of immunoprecipitates from non-transformed wild-type S_3S_{3L} pollen (WT) and transformed pollen expressing *S_{3L}-SLF1:FLAG*, *3-3-L:FLAG* and *H293E:FLAG* mixed with components of the ubiquitination pathway and S_3-RNase and S_{3L}-RNase as substrates (a and b, respectively). Left and right images in each panel show the detection of S-RNase and biotinylated ubiquitin, respectively. Brackets indicate ubiquitinated S-RNase bands observed by two different antibodies. Open arrowheads indicate non-ubiquitinated S-RNases. Arrows indicate ubiquitin monomers. Filled arrowheads indicate the light chain and heavy chain of ubiquitin antibodies.

poly-ubiquitinate S_3-RNases, not S_{3L}-RNases, consistent with the recognition specificity between SLFs and S-RNases: transgenes *S_{3L}-SLF1*, *3-3-L* and *H293E* cause the breakdown of SI in *S_3* pollen, but not in *S_{3L}* pollen, suggesting that S_3-RNases are likely degraded by the proteasome pathway resulting in SI breakdown of *S_3* pollen.

DISCUSSION

The electrostatic potentials act as a major physical force of SLF and S-RNase recognition specificity

Previous studies have shown that the physical interactions between S-RNases and SLFs determine their recognition specificity (Kao and Tsukamoto, 2004; Takayama and Isogai, 2005), but the physical forces between their interactions remains unclear. In this study, we have shown that the alteration of a single C-terminal amino acid of SLF could reverse its surface electrostatic potentials and subsequently the pollen *S* specificity, suggesting that the electrostatic potentials of SLF contributed to the pollen *S* specificity. Based on our results, we propose that the electrostatic potentials of 'like charges repel and unlike charges attract' act as a major physical force between the interactions of SLFs and S-RNases. When S-RNases are recognized by its cognate SLF, their electrostatic repulsions would be generated because of the like electrostatic potentials of the site 293 of SLF and some site of S-RNase in their recognition domain, together with other physical forces such as hydrogen bond and van der Waals interactions generated by additional unknown sites of recognition domain of SLF and S-RNase, thus the recognition domain of S-RNase would not bind to that of SLF, and thus prevent self S-RNase ubiquitination by SCF^{SLF} complex (Figure 6a), and when S-RNases are recognized by a non-self SLF, their electrostatic attraction would be generated to contribute to the specificity because of the opposite electrostatic potentials of the site 293 of SLF and some site of S-RNase in their recognition domain, together with other physical forces such as hydrogen bond and van der Waals interactions generated by some sites of recognition domain of SLF and S-RNase, resulting in the recognition domain of S-RNase binding to that of SLF and non-self S-RNase ubiquitination and degradation (Figure 6b). Our model posits the electrostatic potentials contribute to the SLF recognition specificity in which the recognition domain of S-RNase interact with that of non-self SLF, further supporting the previously proposed S-RNase degradation model and the 'collaborative non-self recognition' system (Kao and McCubbin, 1996; Kao and Tsukamoto, 2004; Zhang *et al.*, 2009; Kubo *et al.*, 2010; Liu *et al.*, 2014). In the 'collaborative non-self recognition' system, each positive or negative charged SLF interacts with a subset of non-self S-RNases with opposite charge and multiple SLF types with positive and negative charges to recognize the entire collection of non-self S-RNases with different charges, but not self S-RNase, suggesting that there must be other physical forces such as hydrogen bond and van der Waals interactions to ensure that all the SLFs within an *S*-haplotype do not recognize self S-RNase. Our model can explain the phenomenon of 'competitive interaction' because the electrostatic potentials of SLFs encoded by two different *S* alleles in a pollen are opposite, positive and negative electrostatic potentials of these SLFs can attract negative and positive of S-RNases, respectively, thus all S-RNases are recognized and degraded leading to compatible response. Nevertheless, the details of this model remain to be further elucidated, for example, what and how other physical forces and which other amino acid(s) on the interaction surface involved in the specificity interactions

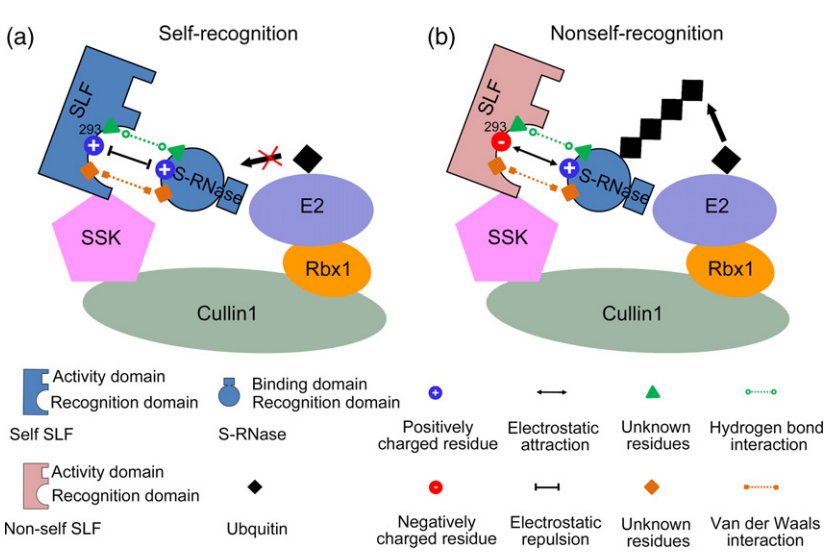

Figure 6. Roles of electrostatic potentials in the physical interactions between SLFs and S-RNases.
(a) Self recognition. When S-RNases are recognized by its cognate SLF, which recruits SLF-interacting SKP1-like1 (SSK1), Cullin 1 (CUL1), and RING-BOX1 (RBX1) to form an SCF^{SLF} complex, their electrostatic repulsion together with other physical forces such as hydrogen bond and van der Waals interactions lead to the binding of the recognition domain S-RNase to that of SLF, and preventing the ubiquitination of self S-RNase by such a functional SCF^{SLF} complex.
(b) Non-self recognition. When S-RNases are recognized by a non-self SLF, their electrostatic attraction together with other physical forces such as hydrogen bond and van der Waals interactions lead to the binding of the recognition domain of S-RNase to that of SLF, and the formation of a functional SCF^{SLF} complex to ubiquitinate non-self S-RNases.

of S-RNases and SLFs besides electrostatic potentials and site 293, and whether there is a threshold value of the electrostatic potentials to discriminate self or non-self recognition. Crystal structure determination of SLF bound to S-RNase would shed light on these issues. To further validate this model, we could alter the amino acids in HV regions of S-RNase affecting the electrostatic potentials, or alter the 293 site of SLF to neutral amino acid such as alanine to test their functions *in vivo*.

Electrostatic force serves as a major mechanism between intracytoplasmic proteins involved in self and non-self recognition

Previous studies have demonstrated that S-RNases and SLFs both are localized in the cytosols of pollen tubes (Takayama and Isogai, 2005; Zhang *et al.*, 2009; Liu *et al.*, 2014), thus their specific recognition must occur in the cytosols. A similar intracytoplasmic protein–protein recognition happens to NBS-LRR and pathogen proteins in plant immune system (Jones and Dangl, 2006; Cui *et al.*, 2015). Plant NBS-LRR proteins directly bind to pathogen virulence proteins or indirectly to a modified host target protein by virulence proteins to recognize effectors. Association with either a modified host protein or a pathogen protein leads to conformational changes in their amino-terminal and LRR domains to achieve specific recognition (Collier and Moffett, 2009). Electrostatic force and hydrophobic interactions also contribute to their specificity recognition. For example, in maize, binding of cofactor NADPH to HCTR1 is mainly governed by van der Waals and nonpolar interactions, whereas binding to HCTR2, electrostatic forces play a dominant role, and the complexes of HC-toxin with HCTR-NADPH are stabilized by a strong network of hydrogen bond and hydrophobic interactions (Dehury *et al.*, 2014). In flax, the polymorphisms in residues of AvrL567 avirulence proteins associated with recognition differences for the R proteins lead to significant changes in surface chemical properties such as surface charge and hydrophobicity, and the specificity recognition results from a cumulative effect of multiple amino acid contacts (Wang *et al.*, 2007). Similarly, our results show that electrostatic potentials significantly contribute to the specific recognition of SLFs and S-RNases, but there appears no evidence to indicate that hydrophobicity contributes to their interactions. Thus, the electrostatic force appears to serve as a major physical mechanism between intracytoplasmic proteins involved in self and non-self recognition. In addition, there are other different mechanisms involved in the recognition of R and pathogen proteins, for example, in pepper, Avr protein binds and activates the promoter of the cognate R gene to achieve specific recognition (Romer *et al.*, 2007). Whether additional mechanisms are involved in the recognition of SLFs and S-RNases needs further investigations.

EXPERIMENTAL PROCEDURES

Plant materials

Self-incompatible *P. hybrida* lines of $S_{3L}S_v$, S_1S_3, and S_3S_3 have been previously described (Robbins *et al.*, 2000; Sims and Ordanic, 2001). Heterozygous S_3S_{3L} was derived from crosses of $S_{3L}S_v \times S_1S_3$.

Protein structure prediction and electrostatic potentials and hydrophobicity analysis

SLF and S-RNase protein structures were modeled using the I-TASSER server (http://zhanglab.ccmb.med.umich.edu/I-TASSER/) (Yang *et al.*, 2015). I-TASSER provides a robust meta-threading alignment for identification of template structures. Take PhS_{3L}-SLF1 for example, the threading programs identified several templates, such as 3mksB (*Saccharomyces cerevisiae* Cdc4/Skp1-SCF-I2), 2ovrB (*Homo sapiens* Skp1-Fbw7-Cyclin E complex), 1nexB (*S. cerevisiae* Skp1-Cdc4-CPD peptide complex), 2vpjA (*H. sapiens* Kelch domain of human KLHL12) and 2e31A (*H. sapiens* Skp1-Fbs1 complex), and generates top five models after iterative simulations. The QMEAN norm score and folding energy of the top five predicted models were calculated by QMEAN server. Backbone conformation and overall model quality of the final refined model were evaluated by the VADAR version1.8 program (http://vadar.wishartlab.com) and the ProSa-web program (https://prosa.services.came.sbg.ac.at/prosa.php) (Willard *et al.*, 2003; Wiederstein and Sippl, 2007). The structure comparison was performed by the Dali server (http://ekhidna.biocenter.helsinki.fi/dali_server/) (Holm and Rosenstrom, 2010). The structures of point-mutated SLFs were generated by Mutagenesis in PyMol. All the structural images were produced by using the PyMol molecular visualization package (L.L.C. Schrodinger, unpublished data). For analysis of electrostatic potentials of predicted SLF and S-RNase proteins, PyMol plug-in APBS tools were applied (Baker *et al.*, 2001), and PDB2PQR and default grid settings were applied for the calculations. For analysis of surface hydrophobicity, CHIMERA software was applied (Pettersen *et al.*, 2004).

Yeast two-hybrid assays

The C-terminal sequences of PhS_3-*SLF1* and PhS_{3L}-*SLF1* (151-1170 bp) were separately introduced into *pGBKT7* vector (Clontech, Mountain View, CA, USA, https://www.clontech.com/) to produce fusion proteins with the GAL4 activation domain. The hypervariable regions of PhS_3-*RNase* (205–336 bp) and PhS_{3L}-*RNase* (205–333 bp) were separately introduced into *pGADT7* vector (Clontech) to form recombinants with the GAL4 DNA-binding domain. The various combinations of BD and AD vectors were co-transformed into yeast strain AH109 and grown on SD/-Leu-Trp medium at 30°C for 3–4 days. The clones were subsequently grown on SD/-Ade-His-Leu-Trp medium at 30°C for 7 days to test interaction.

Generation of Ti plasmid constructs and plant transformation

Eight chimeric genes, *L-3-3*, *3-L-L*, *3-L-3*, *L-3-L*, *3-3-L*, *L-L-3*, *H293E* and *E293H* were constructed by overlap extension PCR, and an *Xba*I restriction site and a *Sac*I site were introduced at the 5′ end and the 3′ end, respectively. A native promoter of PhS_3*A-SLF1* was previously demonstrated that can drive the specific expression of *SLF* genes in pollen, and *Hin*dIII and *Xba*I double-digested

PhS$_3$A-SLF1 native promoter fragment was previously ligated to *pBI101*(Liu *et al.*, 2014). The primers used for this work are listed in Table S8. Then *GUS* gene in *pBI101* was removed, and *Xba*I and *Sac*I double-digested chimeric *SLF* fragments and *S$_{3L}$-SLF1*, *3-3-L*, and *H293E* followed by a sequence encoding FLAG were inserted into *pBI101* containing the *PhS$_3$A-SLF1* promoter. Ti plasmid constructs were separately electroporated into *Agrobacterium tumefaciens* strain LBA4404 (Invitrogen, Carlsbad, CA, USA, http://www.thermofisher.com/), and transformed into leaf disk of *P. hybrida* of *S$_3$S$_{3L}$* genotype using the method previously described (Lee *et al.*, 1994; Qiao *et al.*, 2004a).

DNA gel blotting analysis

Genomic DNA isolation was performed as previously described (Xue *et al.*, 1996). DNA (10 μg) was digested with *Hin*dIII at 37°C overnight, and the DNA fragments were separated by electrophoresis and transferred onto the positive charged nylon membrance Hybond N+ (Amersham, Buckinghamshire, UK, http://www.gelifesciences.com/). The selective marker *NPTII* was used as probes, and labeled with ^{32}P using the Prime-a-Gene labeling system (Promega, Madison, WI, USA, https://www.promega.com/). The following pre-hybridization, hybridization, and washing of the blot were performed following the protocol of manufacturers.

RT-PCR analysis

Total RNA was prepared as previously described (Lai *et al.*, 2002). The first strand cDNA was synthesized using the SuperScript reverse transcriptase (Invitrogen). The RT-PCR was performed using forward primer to *PhSLF* coding region and reverse primer to 3′UTR of *NOS*-terminator listed in Table S8.

Aniline blue staining of pollen tubes

After self-pollination of eight chimeric SLF transgenic lines and their reciprocal crosses with wild-type *S$_3$S$_{3L}$* plants, the pollinated styles were collected to be fixed in ethanol: glacial acetic acid (3:1) solution, and the aniline blue staining of pollen tubes were performed as previously described (Liu *et al.*, 2014).

Genotyping of progeny

To examine the inheritance of chimeric *SLF* transgenes, genomic PCR was performed using *SLF* transgene forward primer and *NOS*-terminator reverse primer. To determine the *S*-genotype of each progeny of transgenic plants, genomic PCR was performed using primers specific to *S$_3$* and *S$_{3L}$-RNase* genes listed in Table S8.

Evolutionary analysis of SLFs

Twenty-one Type-1 SLF sequences from *P. inflata*, *P. hybrida* and *P. axillaris* and 17 SLFs of *S$_9$* haplotype sequences from *P. hybrida* were used to construct a phylogenetic tree to estimate the selective pressure of each amino acid site of them, respectively. Referring to PhS$_{3L}$-SLF1 sequence, the nonsynonymous-synonymous substitution rate ratio (dN/dS) for site classes (K = 3) and NEB probabilities for three classes and postmean ω and P (ω > 1) were calculated by the maximum likelihood (ML) method implemented in CODEML program of the PAML (Phylogenetic Analysis by Maximum Likelihood) software package (Yang, 2007). dN/dS, denoted omega, is used as a measure of selective pressure at the protein level, with omega >1 indicating positive selection. An (NEB) approach is then used to calculate posterior probabilities that a site comes from the site class with omega >1.

Ubiquitination assay

Mature pollen grains from wild-type (*S$_3$S$_{3L}$*) or transgenic plants (*S$_3$S$_{3L}$/S$_{3L}$-SLF1-FLAG*, *S$_3$S$_{3L}$/3-3-L-FLAG*, *S$_3$S$_{3L}$/H293E-FLAG*) were incubated in liquid pollen germination medium (20 mM MES, 15% PEG4000, 2% sucrose, 0.07% $Ca(NO_3)_2{\cdot}4H_2O$, 0.02% $MgSO_4{\cdot}7H_2O$, 0.01% KNO_3, 0.01% H_3BO_3, pH6.0) at 25°C in the dark, and harvested by centrifuging 1000 ***g*** for 1 min. Pollen tube protein was extracted using 50 mM Tris–HCl buffer, pH 7.4, containing 150 mM NaCl, 1% (v/v) Triton X-100 and protease inhibitor cocktail (EDTA-free, Roche, Basel, Switzerland, https://lifescience.roche.com/) and then incubated with anti-FLAG M2 affinity gel (Sigma-Aldrich, St. Louis, MO, USA, http://www.sigmaaldrich.com/) at 4°C for 2 h. Then, the affinity gel was washed five times with 0.5 ml of the TBS buffer. The washed gel was subjected to an ubiquitination assay, serving as the E3 complex. S$_3$-RNases and S$_{3L}$-RNases, used as substrates, were purified by a Smart chromatography system with mono S PC 1.6/5 column (GE Healthcare, Little Chalfont, UK, http://www.gelifesciences.com/) (Entani *et al.*, 1999). Other components for the ubiquitination reaction, including E1, E2, biotinylated ubiquitin, and ATP, were purchased (Ubiquitinylation kit; Enzo Life Science, Raamsdonksveer, The Netherlands, http://www.enzolifesciences.com/), and the ubiquitination assay was carried out at 37°C for 4–6 h. For detection of S-RNases and ubiquitin by immunoblot, rabbit anti-S-RNase IgGs and monoclonal anti-Ub antibody (Sigma-Aldrich) were used as primary antibodies at a 1:5000 and 1:2000 dilution, respectively, and horseradish peroxidase-conjugated anti-rabbit IgGs or anti-mouse IgGs were used as secondary antibody at a 1:10 000 dilution. Rabbit anti-S-RNase IgGs were produced as preciously described (Zhao *et al.*, 2010).

ACKNOWLEDGEMENTS

We thank Dr Cuimin Liu (Institute of genetics and developmental biology, Chinese Academy of Sciences) for providing technical assistance with S-RNase purification experiments and Dr Thomas L. Sims (Northern Illinois University, USA) and Dr Timothy P. Robbins (University of Nottingham, UK) for generously supplying self-incompatible lines of *P. hybrida.* This work was supported by the National Basic Research Program of China (2013CB945102) and the National Natural Science Foundation of China (31221063 and 31401045).

CONFLICT OF INTEREST

The authors declare no competing financial interests.

SUPPORTING INFORMATION

Additional Supporting Information may be found in the online version of this article.

Figure S1. Assessment of the modeled structure of PhS$_3$-RNase.
Figure S2. Assessment of the modeled structure of PhS$_{3L}$-SLF1.
Figure S3. Surface hydrophobicity of SLF and S-RNase proteins.
Figure S4. Schematic representations of six chimeric *SLF* gene constructs and molecular identification of their T$_0$ transgenic lines.
Figure S5. Aniline blue staining analysis of pollen tube growth after reciprocal pollinations between T$_0$ transgenic lines of four domain-swapped constructs and *S$_3$S$_{3L}$* wild-type plants.
Figure S6. Genotyping of T$_1$ progeny from the transgenic plants of *S$_3$S$_{3L}$/3-L-L.*
Figure S7. Genotyping of T$_1$ progeny from the transgenic plants of *S$_3$S$_{3L}$/3-L-3.*
Figure S8. Genotyping of T$_1$ progeny from the transgenic plants of *S$_3$S$_{3L}$/L-3-L.*

Figure S9. Genotyping of T_1 progeny from the transgenic plants of *S_3S_{3L}/3-3-L.*

Figure S10. Phylogenetic tree of Type-1 and *S_9* haplotype SLFs from *Petunia* used to analyse the positive selection of amino acid site of SLF proteins.

Figure S11. Selective pressures on each amino acid site of Type-1 SLF proteins.

Figure S12. Schematic representations of two point-mutated *SLF* constructs and molecular identification of their T_0 transgenic lines.

Figure S13. Aniline blue staining analysis of pollen tube growth after reciprocal pollinations between T_0 transgenic lines of two site mutated *SLFs* constructs and *S_3S_{3L}* wild-type plants.

Figure S14. Genotyping of T_1 progeny from the transgenic plants of *S_3S_{3L}/H293E.*

Figure S15. Genotyping of T_1 progeny from the transgenic plants of *S_3S_{3L}/E293H.*

Figure S16. Selective pressures on each amino acid site of SLF proteins of *S_9* haplotype.

Figure S17. Surface electrostatic potentials of SLF and S-RNase proteins from *P. hybrida* and *P. axillaris.*

Figure S18. Surface electrostatic potentials of SLF and S-RNase proteins from *P. inflata.*

Figure S19. Expression of FLAG-tagged S_{3L}-SLF1, 3-3-L and H293E in pollen of *S_3S_{3L}* heterozygote.

Table S1. The top five predicted models for PhS_{3L}-SLF1 by the I-TASSER suite.

Table S2. Results of self-pollination and the transgene expression of T_0 transgenic lines of six domain-swapped *SLFs.*

Table S3. Analyses of progeny of transformants of the chimeric SLFs that exhibited breakdown of SI.

Table S4. Type-1 and *S_9* haplotype SLF sequences used in evolutionary analysis of SLFs and other SLF and S-RNase sequences used in the experiments.

Table S5. Results of self-pollination and the transgene expression of T_0 transgenic lines of two site mutated *SLFs.*

Table S6. Analyses of progeny of the transformants of point-mutated SLFs that exhibited breakdown of SI.

Table S7. Summary of the relationships of the electrostatic potentials of SLF and S-RNase proteins shown in Figure S17 and S18 and their physical interactions.

Table S8. List of primer sequences shown from 5′ to 3′.

REFERENCES

Aguiar, B., Vieira, J., Cunha, A.E., Fonseca, N.A., Iezzoni, A., van Nocker, S. and Vieira, C.P. (2015) Convergent evolution at the gametophytic self-incompatibility system in *Malus* and *Prunus*. *PLoS ONE*, **10**, e0126138.

Akagi, T., Henry, I.M., Morimoto, T. and Tao, R. (2016) Insights into the *Prunus*-specific S-RNase-based self-incompatibility system from a genome-wide analysis of the evolutionary radiation of *S* locus-related F-box genes. *Plant Cell Physiol.* **57**, 1281–1294.

Ashkani, J. and Rees, D.J. (2016) A comprehensive study of molecular evolution at the self-incompatibility locus of rosaceae. *J. Mol. Evol.* **82**, 128–145.

Baker, N.A., Sept, D., Joseph, S., Holst, M.J. and McCammon, J.A. (2001) Electrostatics of nanosystems: application to microtubules and the ribosome. *Proc. Natl Acad. Sci. USA* **98**, 10037–10041.

Boehm, T. (2006) Quality control in self/nonself discrimination. *Cell*, **125**, 845–858.

Brisolara-Correa, L., Thompson, C.E., Fernandes, C.L. and de Freitas, L.B. (2015) Diversification and distinctive structural features of S-RNase alleles in the genus *Solanum*. *Mol. Genet. Genomics* **290**, 987–1002.

Chanphai, P., Bekale, L. and Tajmir-Riahi, H.A. (2015) Effect of hydrophobicity on protein-protein interactions. *Eur. Polym. J.* **67**, 224–231.

Collier, S.M. and Moffett, P. (2009) NB-LRRs work a 'bait and switch' on pathogens. *Trends Plant Sci.* **14**, 521–529.

Cui, H., Tsuda, K. and Parker, J.E. (2015) Effector-triggered immunity: from pathogen perception to robust defense. *Annu. Rev. Plant Biol.* **66**, 487–511.

De Nettancourt, D. (2001) *Incompatibility and Incongruity in Wild and Cultivated Plants*, 2nd edn. Heidelberg: Springer.

Dehury, B., Patra, M.C., Maharana, J., Sahu, J., Sen, P., Modi, M.K., Choudhury, M.D. and Barooah, M. (2014) Structure-based computational study of two disease resistance gene homologues (*Hm1* and *Hm2*) in maize (*Zea mays* L.) with implications in plant–pathogen interactions. *PLoS ONE*, **9**, e97852.

Entani, T., Takayama, S., Iwano, M., Shiba, H., Che, F.S. and Isogai, A. (1999) Relationship between polyploidy and pollen self-incompatibility phenotype in *Petunia hybrida Vilm*. *Biosci. Biotechnol. Biochem.* **63**, 1882–1888.

Entani, T., Kubo, K., Isogai, S., Fukao, Y., Shirakawa, M., Isogai, A. and Takayama, S. (2014) Ubiquitin-proteasome-mediated degradation of S-RNase in a solanaceous cross-compatibility reaction. *Plant J.* **78**, 1014–1021.

Foote, H.C., Ride, J.P., Franklin-Tong, V.E., Walker, E.A., Lawrence, M.J. and Franklin, F.C. (1994) Cloning and expression of a distinctive class of self-incompatibility (*S*) gene from *Papaver rhoeas* L. *Proc. Natl Acad. Sci. USA* **91**, 2265–2269.

Franklin-Tong, V.E. (2008) *Self-Incompatibility in Flowering Plants*. Heidelberg: Springer.

Holm, L. and Rosenstrom, P. (2010) Dali server: conservation mapping in 3D. *Nucleic Acids Res.* **38**, W545–W549.

Hoseki, J., Ushioda, R. and Nagata, K. (2010) Mechanism and components of endoplasmic reticulum-associated degradation. *J. Biochem.* **147**, 19–25.

Hua, Z., Meng, X. and Kao, T.H. (2007) Comparison of *Petunia inflata S*-Locus F-box protein (Pi SLF) with Pi SLF like proteins reveals its unique function in S-RNase-based self-incompatibility. *Plant Cell*, **19**, 3593–3609.

Ida, K., Norioka, S., Yamamoto, M., Kumasaka, T., Yamashita, E., Newbigin, E., Clarke, A.E., Sakiyama, F. and Sato, M. (2001) The 1.55 D resolution structure of *Nicotiana alata* S_{F11}-RNase associated with gametophytic self-incompatibility. *J. Mol. Biol.* **314**, 103–112.

Ikeda, K., Igic, B., Ushijima, K., Yamane, H., Hauck, N.R., Nakano, R., Sassa, H., Iezzoni, A.F., Kohn, J.R. and Tao, R. (2004) Primary structural features of the *S* haplotype-specific F-box protein, SFB, in *Prunus*. *Sex. Plant Reprod.* **16**, 235–243.

Jones, J.D.G. and Dangl, J.L. (2006) The plant immune system. *Nature*, **444**, 323–329.

Jones, S. and Thornton, J.M. (1996) Principles of protein-protein interactions. *Proc. Natl Acad. Sci. USA* **93**, 13–20.

Kao, T.H. and McCubbin, A.G. (1996) How flowering plants discriminate between self and non-self pollen to prevent inbreeding. *Proc. Natl Acad. Sci. USA* **93**, 12059–12065.

Kao, T.H. and Tsukamoto, T. (2004) The molecular and genetic bases of S-RNase-based self-incompatibility. *Plant Cell*, **16**(Suppl), S72–S83.

Kubo, K., Entani, T., Takara, A. *et al.* (2010) Collaborative non-self recognition system in S-RNase-based self-incompatibility. *Science*, **330**, 796–799.

Lai, Z., Ma, W., Han, B., Liang, L., Zhang, Y., Hong, G. and Xue, Y. (2002) An F-box gene linked to the self-incompatibility (*S*) locus of *Antirrhinum* is expressed specifically in pollen and tapetum. *Plant Mol. Biol.* **50**, 29–42.

Lee, H.S., Huang, S. and Kao, T.H. (1994) *S* proteins control rejection of incompatible pollen in *Petunia inflata*. *Nature*, **367**, 560–563.

Liu, W., Fan, J., Li, J., Song, Y., Li, Q., Zhang, Y. and Xue, Y. (2014) SCF^{SLF}-mediated cytosolic degradation of S-RNase is required for cross-pollen compatibility in S-RNase-based self-incompatibility in *Petunia hybrida*. *Front. Genet.* **5**, 228.

Matsuura, T., Sakai, H., Unno, M., Ida, K., Sato, M., Sakiyama, F. and Norioka, S. (2001) Crystal structure at 1.5-A° resolution of *Pyrus pyrifolia* pistil ribonuclease responsible for gametophytic self-incompatibility. *J. Biol. Chem.* **276**, 45261–45269.

Matton, D.P., Maes, O., Laublin, G., Xike, Q., Bertrand, C., Morse, D. and Cappadocia, M. (1997) Hypervariable domains of self-incompatibility RNases mediate allele-specific pollen recognition. *Plant Cell*, **9**, 1757–1766.

Matton, D.P., Luu, D.T., Xike, Q., Laublin, G., O'Brien, M., Maes, O., Morse, D. and Cappadocia, M. (1999) Production of an S-RNase with dual specificity suggests a novel hypothesis for the generation of new *S* alleles. *Plant Cell*, **11**, 2087–2097.

Mizushima, T., Yoshida, Y., Kumanomidou, T., Hasegawa, Y., Suzuki, A., Yamane, T. and Tanaka, K. (2007) Structural basis for the selection of glycosylated substrates by SCF^{Fbs1} ubiquitin ligase. *Proc. Natl Acad. Sci. USA* **104**, 5777–5781.

Murfett, J., Atherton, T.L., Mou, B., Gasser, C.S. and McClure, B.A. (1994) S-RNase expressed in transgenic *Nicotiana* causes *S*-allele-specific pollen rejection. *Nature*, **367**, 563–566.

Newbigin, E., Paape, T. and Kohn, J.R. (2008) RNase-based self-incompatibility: puzzled by pollen *S*. *Plant Cell*, **20**, 2286–2292.

Nunes, M.D., Santos, R.A., Ferreira, S.M., Vieira, J. and Vieira, C.P. (2006) Variability patterns and positively selected sites at the gametophytic self-incompatibility pollen SFB gene in a wild self-incompatible *Prunus spinosa* (Rosaceae) population. *New Phytol.* **172**, 577–587.

Parham, P. and Moffett, A. (2013) Variable NK cell receptors and their MHC class I ligands in immunity, reproduction and human evolution. *Nat. Rev. Immunol.* **13**, 133–144.

Pettersen, E.F., Goddard, T.D., Huang, C.C., Couch, G.S., Greenblatt, D.M., Meng, E.C. and Ferrin, T.E. (2004) UCSF Chimera—a visualization system for exploratory research and analysis. *J. Comput. Chem.* **25**, 1605–1612.

Qiao, H., Wang, F., Zhao, L., Zhou, J., Lai, Z., Zhang, Y., Robbins, T.P. and Xue, Y. (2004a) The F-box protein AhSLF-S_2 controls the pollen function of S-RNase-based self-incompatibility. *Plant Cell*, **16**, 2307–2322.

Qiao, H., Wang, H., Zhao, L., Zhou, J., Huang, J., Zhang, Y. and Xue, Y. (2004b) The F-box protein AhSLF-S_2 physically interacts with S-RNases that may be inhibited by the ubiquitin/26S proteasome pathway of protein degradation during compatible pollination in *Antirrhinum*. *Plant Cell*, **16**, 582–595.

Robbins, T.P., Harbord, R.M., Sonneveld, T. and Clarke, K. (2000) The molecular genetics of self-incompatibility in *Petunia hybrida*. *Ann. Bot.* **85**, 105–112.

Romer, P., Hahn, S., Jordan, T., Strauss, T., Bonas, U. and Lahaye, T. (2007) Plant pathogen recognition mediated by promoter activation of the pepper *Bs3* resistance gene. *Science*, **318**, 645–648.

Rossjohn, J., Gras, S., Miles, J.J., Turner, S.J., Godfrey, D.I. and McCluskey, J. (2015) T cell antigen receptor recognition of antigen-presenting molecules. *Annu. Rev. Immunol.* **33**, 169–200.

Rudolph, M.G. and Wilson, I.A. (2002) The specificity of TCR/pMHC interaction. *Curr. Opin. Immunol.* **14**, 52–65.

Rudolph, M.G., Stanfield, R.L. and Wilson, I.A. (2006) How TCRs bind MHCs, peptides, and coreceptors. *Annu. Rev. Immunol.* **24**, 419–466.

Sassa, H., Kakui, H., Miyamoto, M., Suzuki, Y., Hanada, T., Ushijima, K., Kusaba, M., Hirano, H. and Koba, T. (2007) *S* locus F-box brothers: multiple and pollen-specific F-box genes with *S* haplotype-specific polymorphisms in apple and Japanese pear. *Genetics*, **175**, 1869–1881.

Schopfer, C.R., Nasrallah, M.E. and Nasrallah, J.B. (1999) The male determinant of self-incompatibility in *Brassica*. *Science*, **286**, 1697–1700.

Schwessinger, B. and Ronald, P.C. (2012) Plant innate immunity: perception of conserved microbial signatures. *Annu. Rev. Plant Biol.* **63**, 451–482.

Sijacic, P., Wang, X., Skirpan, A.L., Wang, Y., Dowd, P.E., McCubbin, A.G., Huang, S. and Kao, T.H. (2004) Identification of the pollen determinant of S-RNase-mediated self-incompatibility. *Nature*, **429**, 302–305.

Sims, T.L. and Ordanic, M. (2001) Identification of a *S*-ribonuclease-binding protein in *Petunia hybrida*. *Plant Mol. Biol.* **47**, 771–783.

Skaar, J.R., Pagan, J.K. and Pagano, M. (2013) Mechanisms and function of substrate recruitment by F-box proteins. *Nat. Rev. Mol. Cell Biol.* **14**, 369–381.

Sudha, G., Nussinov, R. and Srinivasan, N. (2014) An overview of recent advances in structural bioinformatics of protein-protein interactions and a guide to their principles. *Prog. Biophys. Mol. Biol.* **116**, 141–150.

Takasaki, T., Hatakeyama, K., Suzuki, G., Watanabe, M., Isogai, A. and Hinata, K. (2000) The *S* receptor kinase determines self-incompatibility in *Brassica* stigma. *Nature*, **403**, 913–916.

Takayama, S. and Isogai, A. (2005) Self-incompatibility in plants. *Annu. Rev. Plant Biol.* **56**, 467–489.

Takayama, S., Shimosato, H., Shiba, H., Funato, M., Che, F.S., Watanabe, M., Iwano, M. and Isogai, A. (2001) Direct ligand-receptor complex interaction controls *Brassica* self-incompatibility. *Nature*, **413**, 534–538.

Ushijima, K., Sassa, H., Dandekar, A.M., Gradziel, T.M., Tao, R. and Hirano, H. (2003) Structural and transcriptional analysis of the self-incompatibility locus of almond: identification of a pollen-expressed F-box gene with haplotype-specific polymorphism. *Plant Cell*, **15**, 771–781.

Vieira, J., Morales-Hojas, R., Santos, R.A. and Vieira, C.P. (2007) Different positively selected sites at the gametophytic self-incompatibility pistil S-RNase gene in the Solanaceae and Rosaceae (*Prunus*, *Pyrus*, and *Malus*). *J. Mol. Evol.* **65**, 175–185.

Wang, C.I., Guncar, G., Forwood, J.K. *et al.* (2007) Crystal structures of flax rust avirulence proteins AvrL567-A and -D reveal details of the structural basis for flax disease resistance specificity. *Plant Cell*, **19**, 2898–2912.

Wheeler, M.J., de Graaf, B.H., Hadjiosif, N., Perry, R.M., Poulter, N.S., Osman, K., Vatovec, S., Harper, A., Franklin, F.C. and Franklin-Tong, V.E. (2009) Identification of the pollen self-incompatibility determinant in *Papaver rhoeas*. *Nature*, **459**, 992–995.

Wiederstein, M. and Sippl, M.J. (2007) ProSA-web: interactive web service for the recognition of errors in three-dimensional structures of proteins. *Nucleic Acids Res.* **35**, W407–W410.

Willard, L., Ranjan, A., Zhang, H., Monzavi, H., Boyko, R.F., Sykes, B.D. and Wishart, D.S. (2003) VADAR: a web server for quantitative evaluation of protein structure quality. *Nucleic Acids Res.* **31**, 3316–3319.

Williams, J.S., Natale, C.A., Wang, N., Li, S., Brubaker, T.R., Sun, P. and Kao, T.H. (2014) Four previously identified *Petunia inflata S*-locus F-box genes are involved in pollen specificity in self-incompatibility. *Mol. Plant* **7**, 567–569.

Xue, Y., Carpenter, R., Dickinson, H.G. and Coen, E.S. (1996) Origin of allelic diversity in *Antirrhinum S* locus RNases. *Plant Cell*, **8**, 805–814.

Yang, Z. (2007) PAML 4: phylogenetic analysis by maximum likelihood. *Mol. Biol. Evol.* **24**, 1586–1591.

Yang, J., Yan, R., Roy, A., Xu, D., Poisson, J. and Zhang, Y. (2015) The I-TASSER Suite: protein structure and function prediction. *Nat. Methods* **12**, 7–8.

Zhang, Y., Zhao, Z. and Xue, Y. (2009) Roles of proteolysis in plant self-incompatibility. *Annu. Rev. Plant Biol.* **60**, 21–42.

Zhang, Z., Witham, S. and Alexov, E. (2011) On the role of electrostatics in protein-protein interactions. *Phys. Biol.* **8**, 035001.

Zhao, L., Huang, J., Zhao, Z., Li, Q., Sims, T.L. and Xue, Y. (2010) The Skp1-like protein SSK1 is required for cross-pollen compatibility in S-RNase-based self-incompatibility. *Plant J.* **62**, 52–63.

Zhou, J.L., Wang, F., Ma, W.S., Zhang, Y.S., Han, B. and Xue, Y.B. (2003) Structural and transcriptional analysis of *S*-locus F-box genes in *Antirrhinum*. *Sex. Plant Reprod.* **16**, 165–177.

